High Resolution Microsphere-Assisted Interference Microscopy for 3D Characterization of Nanomaterials

Audrey Leong-Hoi, Camille Hairaye, Stephane Perrin, Sylvain Lecler, Pierre Pfeiffer, and Paul Montgomery*

Nanoscale materials are nowadays widely used in many different modern technologies. Special attention is thus required for their characterization in order to optimize fabrication processes. However, current characterization systems which can achieve nanometric resolution over a large area and in three dimensions are few. Classical optical microscopy presents a resolving power limited by diffraction, making impossible the visualization of elements with a size under half the wavelength. Recently, several methods have thus been developed to overcome this limitation, among them microsphere-assisted microscopy. Indeed, using a transparent microsphere, a full-field image of the sample can be retrieved with a higher resolution than the diffraction-limit. In this paper, this new imaging technique is combined with phase-shifting interferometry in order to reconstruct the 3D surface of nanostructures. An enhancement of a factor of 4.0 in the lateral resolution is demonstrated while combining this with the nanometric axial sensitivity of interferometry. Results are shown of the topography of reference gratings as well as periodic Ag nano-dots on silicon and laser induced ripples in steel, spaced by a few hundred nanometres. A comparison of these results is made with those from SEM and atomic force microscopy.

1. Introduction

The characterization of nanoscale features which are present in micro-electronic devices, in microsystems and in surface coatings of materials, is a significant challenge. Indeed, their sub-wavelength size and their complex layers can introduce errors in measurements. Currently, techniques exist for characterizing them such as atomic force microscopy (AFM), scanning electron microscopy (SEM), ellipsometry, etc. However, they often present the inconveniences of either being expensive, requiring a long-acquisition time through a lateral scanning over the field of view or elaborate sample preparation.

Interference microscopy has become a reference for the characterization of materials,[1] using white light interferometry[2] or quantitative phase-contrast interferometry[3] for the surface analysis of samples, and full-field optical coherence tomography[4] for volume inspection. These optical metrology techniques provide a large field of view acquisition and a fast reconstruction of the sample. Furthermore, a high axial sensitivity (better than 1 nm on smooth surfaces) over a large depth of field is achieved.[5] However, the diffraction of the light limits the lateral resolution of interference microscopes. Assuming incoherent illumination, the size of the smallest discernible object cannot be higher than half of the central wavelength of the light source in air, that is 200 nm.[6] This limitation results in an inhomogeneity in the three-dimensional resolution. Indeed, the lateral resolution of an interference microscope is over two orders of magnitude worse than the axial resolution.[7]

Over the last two decades, many methods have been developed in order to overcome the physical barrier of diffraction and thus to perform far-field optical nanoscale imaging. Working in immersion allows the enhancement of the resolution through an increase in the numerical aperture of the system. Nevertheless, the resolution is still insufficient for smaller structures. In 2005 and, further, in 2009, two new imaging techniques, that is structured illumination microscopy[8] and tomographic diffraction microscopy,[9] were developed specifically for 3D measurement. Both are based on the generation of a larger synthetic numerical aperture.

Inspired by the work on photonic-jet-based scanning microscopy,[10,11] Wang et al. demonstrated experimentally full-field microsphere-assisted microscopy.[12] Introducing a transparent microsphere in a classical microscope allows overcoming the diffraction limit through the collection of the evanescent wave information. It is thought that placing the

Dr. A. Leong-Hoi, Dr. C. Hairaye, Dr. S. Perrin, Dr. S. Lecler,
Dr. P. Pfeiffer, Dr. P. Montgomery
ICube
University of Strasbourg, UMR CNRS 7357
300 Boulevard Sébastien Brand, 67412 Illkirch, France
E-mail: aleonghoi@unistra.fr

Dr. C. Hairaye
IREPA LASER
Institut Carnot MICA
Parc d'Innovation
320 Boulevard Sébastien Brant, 67400 Illkirch, France

DOI: 10.1002/pssa.201700858

microsphere on the sample allows the conversion of the near-field waves into far-field propagating waves. Lateral resolutions of 100 nm, in air, and 50 nm, in water, were reported.[12,13] In order to perform non-invasive acquisitions, recent work has shown that the microsphere can also be placed in a contactless configuration with the object while keeping the super-resolution.[14]

The microsphere acts as a magnification optical component which provides a virtual image of the object, as shown in **Figure 1**. Then, a microscope objective collects the magnified virtual image. Different microsphere materials can be employed such as silica glass or barium titanate, depending on whether it is used in air or in water. Another main advantage of this technique is that it does not need sample labelling.

In 2016, Wang et al. applied microsphere-assisted microscopy to coherence scanning interference microscopy[15] using a Linnik configuration, achieving a lateral resolution of 60 nm in immersion. At the same time, Kassamakov et al. implemented a Mirau-based microsphere-assisted microscope in air.[16] In 2017, a digital holographic microscope assisted by microsphere was developed for precise cell identification.[17] Finally, a microsphere-assisted phase-shifting microscope (MAPS) was implemented for improving the lateral resolution of 3D measurements.[18]

In this paper, the MAPS technique is applied to the 3D characterization of nano-features and the reconstruction of nanomaterial topography. The results have been performed on silicon reference gratings, on periodic Ag nanodots on silicon, and on laser induced nanometric ripples obtained on stainless-steel. The topographic measurements have been retrieved using low coherence illumination and a 24-µm diameter soda lime glass microsphere in air. Furthermore, they are compared to the surface reconstruction using the collecting objective alone. A lateral resolution improvement by a factor of 4.0 has been demonstrated using the MAPS nanoscopy system.

2. Microsphere-Assisted Microscopy

Recently, a numerical analysis of the performances of the microsphere-assisted microscopy technique through rigorous simulations has been reported in Ref. [19]. Despite the phenomenon at the root of the super-resolution effect being currently not fully understood, the results of these simulations show the importance of the geometrical and optical parameters on the magnification and on the lateral resolution improvement. A magnification factor of 4.0, leading to a lateral resolution of 250 nm, has been reported using a 20-µm diameter soda lime glass microsphere with a white light source centred at 500 nm. This result agrees with the experimental measurements shown in **Figure 2** where the diameter of the microspheres is around 24 µm (cf. Figure 2(a)). Here, the sample is a 400-nm period grating. The microscope objective (X50, NA = 0.55) alone cannot resolve the features of the object. Indeed, according to Fourier optics, the resolving power of the diffraction-limited microscope equals 450 nm in this case.

In contrast, microsphere-assisted microscopy does allow measuring the sample by focusing through the microsphere, as shown in Figure 2(b). The virtual image of the 400-nm period grating is magnified, giving a measured period of 1.52 µm. The magnification of 3.8 thus induced by the microsphere is the ratio between the measured period (1.52 µm) and the nominal period (0.4 µm) of the grating. This magnification experimentally obtained is in agreement with the simulations described in Ref. [19]. In this work, a 24-µm diameter soda lime glass microsphere has been used since this gives a good compromise between lateral field of view and resolution that the MAPS technique provides. Indeed, the geometrical parameters of the microsphere as well as the optical parameters of the light source, have to be considered in the evaluation of the performance of the imaging technique,[14,19] for example the lower is the microsphere size, the higher is the lateral resolution. However, as the field of view through a microsphere is about a fifth of its diameter, a larger microsphere size leads to a higher lateral field of view.

3. Microsphere-Assisted Profilometry

To perform a three-dimension measurement of the surface topography of the sample, phase-shifting interferometry is employed.[18] In this work, the reflective interferometric setup is

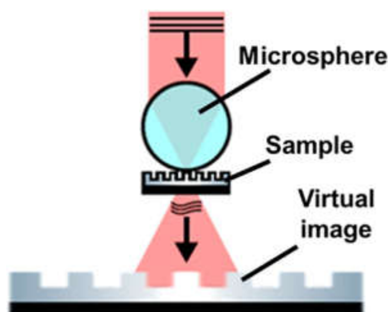

Figure 1. Principle of microsphere-assisted microscopy. A white light source illuminates the sample through a microsphere placed onto it. An objective is used to collect the virtual image of the sample.

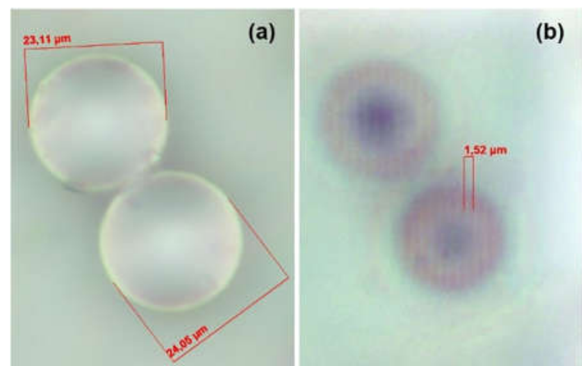

Figure 2. (a) Image of the microspheres used, obtained with a classical microscope with X50 objective (NA = 0.55) and (b) imaging of a 400-nm period grating through the 24-µm diameter microspheres (with refractive index of 1.5). The illumination is a white light source. The magnification of the microsphere is 3.8.

based on the Linnik interferometric configuration which consists of two perpendicular arms, as shown in **Figure 3**.

The incident beam from the white light source is divided into two beams, that is the reference and the object arms, by the beam splitter cube. In the reference arm, the beam passes through a microscope objective MO (X50, NA = 0.3) and is then back-reflected by the reference mirror to be collected by the MO. The position of the components of the reference arm is then adjusted to balance the two arms of the interferometer due to the presence of the microsphere. In the object arm, the light beam illuminates the sample with a similar MO and the soda lime silica glass microsphere (diameter of 24 μm and refractive index of 1.5). Then, the MO collects the virtual image of the sample provided by the microsphere as in Figure 2(b). Interference occurs when the optical path difference (OPD) between the two arms is inferior to the coherence length of the light source. The piezo-electric device supporting the sample, allows the application of the phase-shift between the two arms of the interferometer. The five-step algorithm is used with a phase shift of $\pi/2$.[1] Finally, the beam splitter cube combines the two beams and the CMOS camera records the interference through the tube lens.

To evaluate the height of the features of the sample, the phase reconstruction is first digitally unwrapped[20] and then

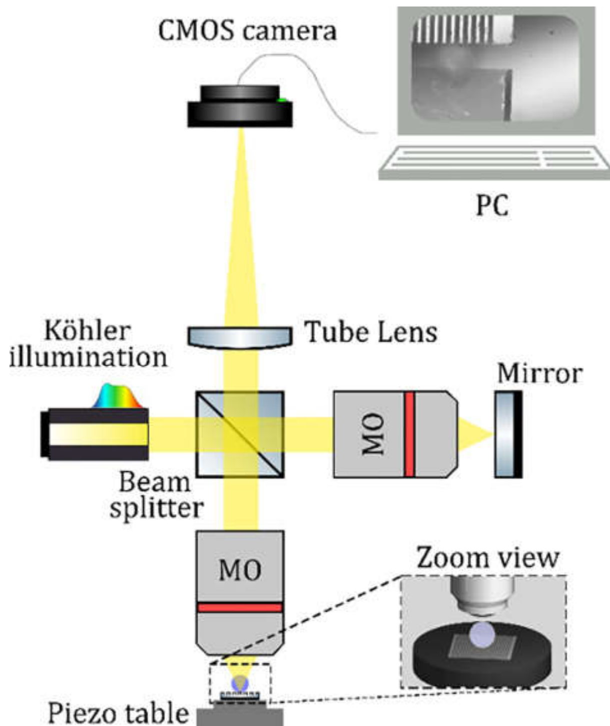

Figure 3. Layout of the experimental setup based on a Linnik configuration. The object arm consists of the microscope objective MO to collect the virtual image generated by the microsphere, the sample, and the piezo-actuator device. A similar MO and a reference mirror make up the reference arm. Both are illuminated by a broadband light source with a Köhler arrangement. The interference pattern is recorded by the camera through the tube lens.

converted into an optical path difference (OPD) distribution. However, the spherical microbead yields a non-negligible curved deformation in the measured phase which is removed using a polynomial 2D fit in the image processing process.[18] This correction is achieved by first making a reference measurement of the microsphere deformation on a known flat surface, giving the coefficient of a polynomial function specific to each microsphere. The residual obtained from the fitted model then leads to the deformation-free wavefront.

4. Results and Discussions

The measurements have been performed using two types of light source, that is an incandescent lamp and a white-light LED. Without implementation of the MAPS technique, the lateral resolution of the Linnik interference system is about 1.3 μm with the incandescent lamp and about 900 nm with the white-light LED. Gratings with periods just below 1 μm can therefore hardly be reconstructed in 3D due to the lack of lateral resolution, hence the difficulty of characterizing nanostructures. In order to demonstrate the improvement obtained with the MAPS system, three types of nanomaterials have been used: 400- and 300-nm period silicon gratings, 200–300 nm sized Ag nano-dots covered by a SiON layer obtained by nano imprint lithography, and 900-nm periodic ripples, textured with a femtosecond fibre laser on stainless steel. The surface topography of all these samples has also been measured using a Park XE70 AFM microscope placed in a vibration isolation chamber and working in the non-contact mode. The tip used was a noncontact high frequency point probe with a tip radius of 2 nm and a width of 10 nm at a distance of 100 nm from the tip.

4.1. Resolution Standard Gratings

The reference grating sample used (RS-N gratings from SiMETRICS GmbH) consists of a series of sub-gratings with pitch values varying from 300 to 6 μm. The two fields used are the 400-nm and the 300-nm period gratings that are, as expected, not resolved at all by the Linnik interference microscope directly (without the microsphere).

Figure 4 shows measurements of the 400-nm period grating with AFM and the measured values given by the arrows in the line profile are listed in **Table 1**.

The 3D measurement obtained with the MAPS system in white light ($\lambda = 520$ nm) through a 24 μm diameter glass microsphere (cf. **Figure 5**) shows that the grating is magnified by a factor of 3.65 and gives a measured averaged depth of 24.5 nm, approaching thus the value obtained by AFM revealing a pitch of 406 nm and a total depth of around 95 nm.

Figure 6 shows measurements of the 300-nm period grating with AFM and the measured values given by the arrows in the line profile are listed in **Table 2**. The illumination light source in the MAPS system was then replaced by a lower-wavelength light source ($\lambda = 460$ nm). The 3D measurement obtained through a 24 μm diameter glass microsphere (cf. **Figure 7**)

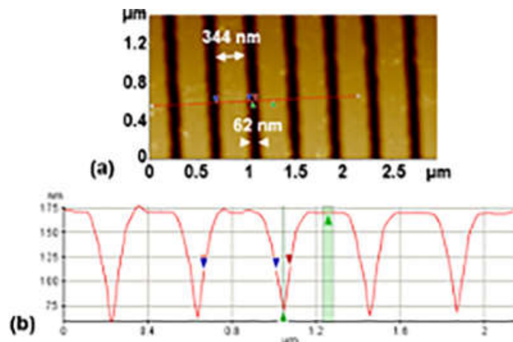

Figure 4. Measurements of the 400-nm period grating with AFM. (a) Surface topography. (b) Profile from (a): the height between green arrows is 95 nm.

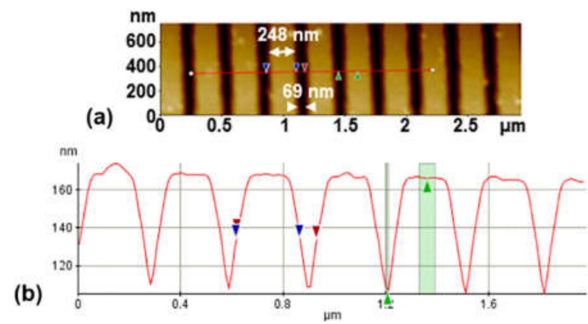

Figure 6. Measurements of the 300-nm period grating with AFM. (a) Surface topography. (b) Profile from (a): the height between green arrows is of 33 nm.

Table 1. Measured values of the arrows in the line profile of **Figure 4**.

Cursor	ΔX (μm)	ΔY (nm)
Red	0.406	0.651
Green	0.212	94.975
Blue	0.344	0.311

Table 2. Measured values of the arrows in the line profile of **Figure 6**.

Cursor	ΔX (μm)	ΔY (nm)
Red	0.317	2.170
Green	0.159	32.792
Blue	0.248	0.060

shows that the grating is magnified by a factor of 4.4 and a measured averaged depth of 27 nm, close to the value obtained by AFM revealing a pitch of 317 nm and a total depth of around 33 nm. It can be noted that the magnification factor in this case is different from that in the measurement in Figure 5 because of the change of the source wavelength which influences the results, that is the magnification and the resolution, as explained in Ref. [18].

Nonetheless the depth profile measured with AFM can be observed to be not square but with sidewalls that appear to be inclined and with a V-shaped structure (cf. Figure 4(b) and Figure 6(b)). The differences in the measured profiles with those through the microsphere could be either due to a lack of lateral resolution in the latter case or to slight variations in the profiles between the different positions measured with the two techniques.

Moreover, a high ratio factor between the height and the width of the grating can reduce significantly the back-reflected signal from the bottom of the grating, leading (in MAPS and in interferometry in general) to measurement errors.

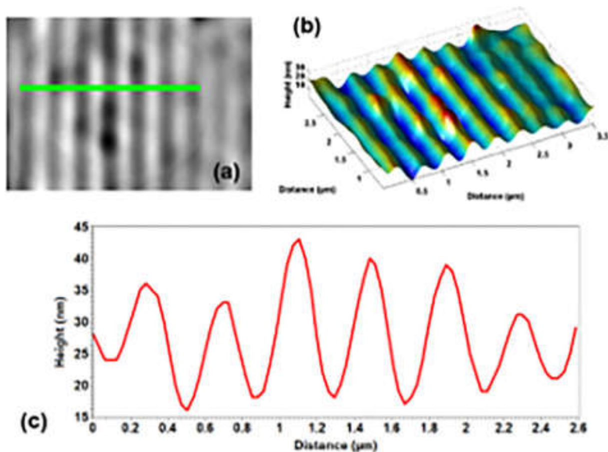

Figure 5. Measurements of the 400-nm period grating with the MAPS system with a 24-μm diameter microsphere. (a) Surface topography and (b) 3D measurement through the microsphere. (c) Profile from (a): the average height is of 24.5 nm.

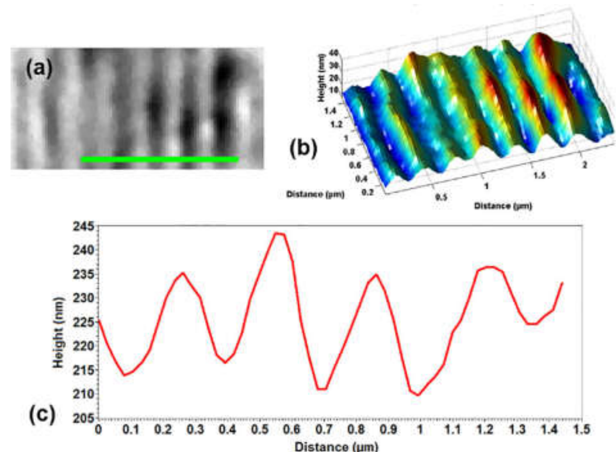

Figure 7. Measurements of the 300-nm period grating with the MAPS system with a 24-μm diameter microsphere. (a) Surface topography and (b) 3D measurement through the microsphere. (c) Profile from (a): the average height is of 27 nm.

4.2. Silver Nano-Dots

This sample consists in an array of silver (Ag) nano-dots covered by a silicon-oxynitride (SiON) layer on silicon made by nano imprint lithography. These nanostructures are used to obtain plasmonic resonance in order to increase the absorption in photovoltaic cells.

AFM measurements were first performed to obtain the size and depth of the nano-dots, as illustrated in **Figure** 8(a) and (b). They are so small (200 nm wide, 300 nm long and 30 nm deep) that they cannot be measured by the Linnik system directly ($\lambda = 560$ nm). Nevertheless, by using a 24-µm diameter glass microsphere with a magnification of 4.4, the virtual image allows the phase shifting technique to be used (cf. Figure 8(c)). After unwrapping the phase image, the height (cf. Figure 8(d)) and the 3D topography (cf. Figure 8(e)) of the nano-dots can be retrieved.

By analyzing the horizontal and vertical profiles, the size and the depth of the nanostructures through the microsphere were then measured. The horizontal profile in Figure 8(f) and (g) shows a width of 200 nm and an average depth of 22.5 nm. The vertical profile in Figure 8(h) and (i) shows a length of 325 nm and an average depth of 25 nm. The measurements obtained with the MAPS system are thus in agreement with those obtained by AFM.

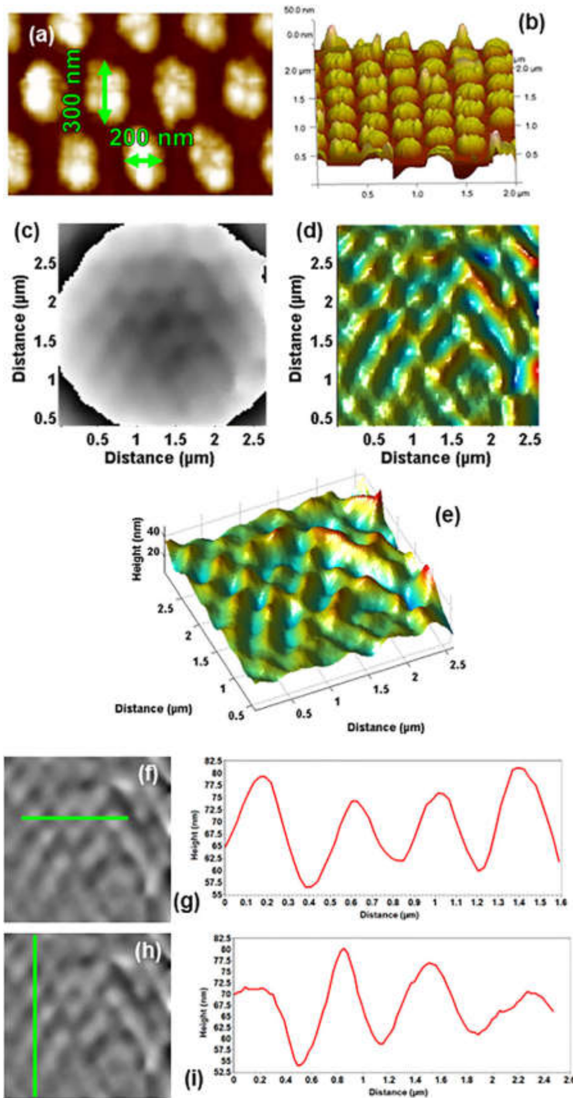

Figure 8. Measurements of the Ag nano-dots using AFM and the MAPS system with a 24-µm diameter microsphere. (a) Surface topography and (b) 3D measurement by AFM. (c) Phase image, (d) topography after unwrapping and (e) 3D surface through the microsphere. (f) Position of the horizontal profile. (g) Profile from (f): the average height is of 22.5 nm. (h) Position of the vertical profile. (i) Profile from (h): the average height is of 25 nm.

4.3. Ripples

The ripples studied are laser-induced periodic surface structures, generated by the self-organization of the metallic material (AISI 316L stainless steel) after irradiation with femtosecond laser pulses. These quasi-periodical structures present a spatial period of the order of the laser wavelength and a preferential orientation perpendicular to the direction of the incident linear polarization.[21–23]

The laser pulses are provided by a diode-pumped Ytterbium fibre laser (Tangerine, Amplitude Systèmes, France), at a central wavelength of 1030 nm, for a duration of 300 fs and a maximal pulse energy of 150 µJ at a repetition rate of 200 kHz. The nanostructures were obtained in a one-step process, with a focused diameter of about 40 µm for a laser fluence of 0.49 J cm^{-2} and a spot overlap of 70% at a repetition rate of 50 kHz. It is possible to modify the orientation of the ripples, by rotating the incident linear polarization thanks to a half-wave plate, added in the optical path of the laser beam.

These nanomaterials are used to change the visual aspect of the textured surface, for applications in traceability, and identification for anti-counterfeiting.[24] A specific interest is the production of a diffractive coloring effect, as shown in **Figure 9**, due to the presence of the ripples on the surface.

SEM and AFM measurements were first performed to obtain the size and depth of the ripples with three different orientations (5°, 30°, and 55°), as illustrated in **Figure 10**. The average period

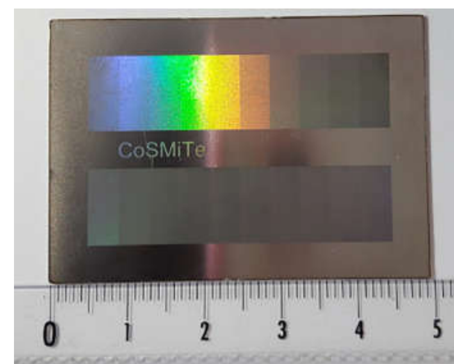

Figure 9. Color effect due to ripples obtained on a stainless steel sample, after irradiation with femtosecond laser pulses.

measured by both these techniques gives values of about 950 nm. The 3D measurements obtained with the Linnik interference system in white light ($\lambda_0 = 800$ nm) directly can hardly be made, showing a much-reduced height of between 10 and 14 nm instead of 280 nm measured with AFM.

By using a 24-µm soda lime glass microsphere ($n = 1.5$), the virtual image magnifies the ripples by a factor of 4, **Figure 11** showing them with and without interference fringes. The phase image is also shown before unwrapping, together with the false color height and 3D images. By analyzing the profiles (cf. Figure 11), it can be noticed that the heights measured with the MAPS system have been slightly improved for the three

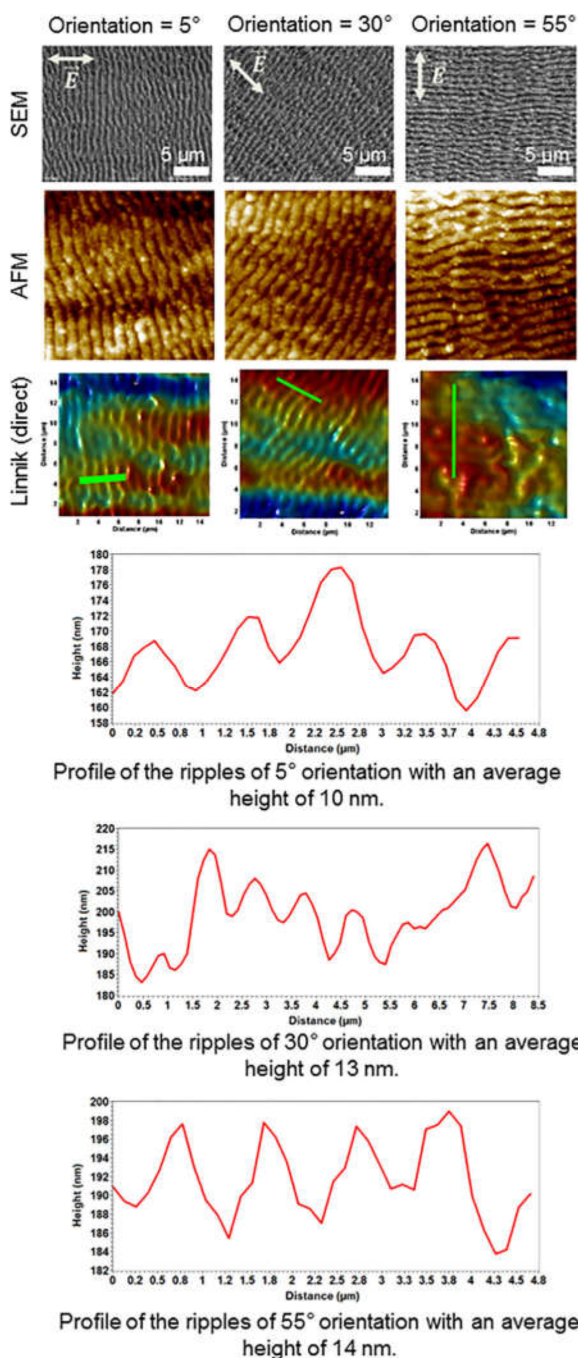

Figure 10. Measurements of the ripples with orientations of 5°, 30°, and 55° using SEM, AFM and the Linnik white light interference microscope in air.

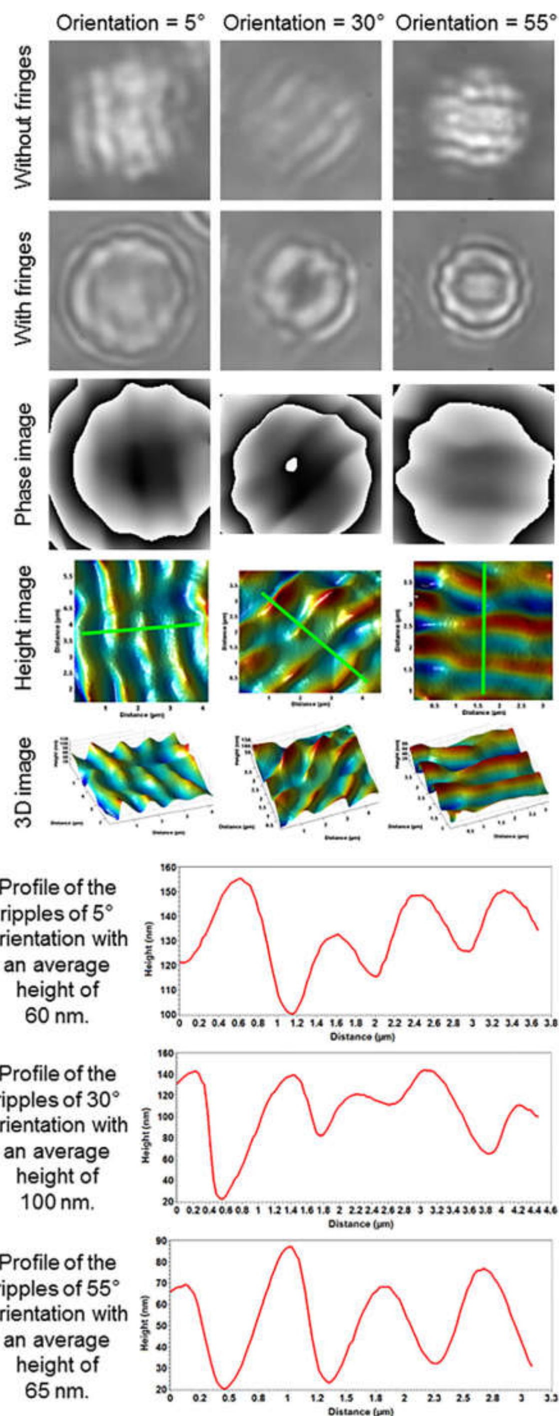

Figure 11. Measurements of the ripples with orientations of 5°, 30°, and 55° using the MAPS system with 24-µm diameter microspheres.

orientations compared with the direct measurements without the microsphere (Figure 10).

However, it can be noticed that height errors still remain, which could be due to the correction of the curved deformation in the measured phase due to the use of the spherical microbead.

5. Conclusion

The new technique of microsphere-assisted phase-shifting white-light interfere microscopy using a Linnik configuration in air has been investigated in the characterization of nano-surfaces. Measurements have been performed on three types of nanomaterials: calibrated resolution standard gratings in silicon, periodic Ag nano-dots on silicon made by nano imprint lithography, and of periodic ripples in stainless steel made by femtosecond laser nanotexturing. The results obtained have demonstrated an improvement by a factor of about 3.65–4.4 in the lateral resolution in air with 24-μm diameter soda lime glass microspheres ($n = 1.5$) in white light.

A more isotropic high resolution is thus achieved for full-field surface profilometry, with the advantages of being in the far field. However, while the lateral resolution is improved with the microsphere-assisted technique, there are nonetheless some artefacts present in the 3D measurements. For example, regions of blurring could be observed in certain experimental results, possibly due to non-optimized illumination conditions or non-uniformity or surface damage to the microspheres.

The results, compared with AFM measurements, confirm nevertheless that lateral super-resolution in interferometry can be performed in a far field 3D optical imaging system using dielectric microspheres placed on the sample below the imaging objective. This new microsphere-assisted technique thus opens new possibilities for high resolution characterization in nanometrology.

Acknowledgements

The authors would like to thank Thomas FIX (ICube, France) for providing the Ag nano-dots sample and Hongyu LI for the image acquisitions in Figure 2. Acknowledgements are extended to the University of Strasbourg and the SATT Conectus Alsace for funding.

Conflict of Interest

The authors declare no conflict of interest.

Keywords

interference microscopy, interferometry, microspheres, nanomaterials

Received: November 8, 2017
Published online:

[1] D. Malacara, *Optical Shop Testing*, John Wiley & Sons, New York **2007**.
[2] J. Schmit, J. Reed, E. Novak, J. K. Gimzewski, *J. Opt. A: Pure Appl. Opt*. **2008**, *10*, 064001.
[3] E. Cuche, F. Bevilacqua, C. Depeursinge, *Opt. Lett*. **1999**, *24*, 291.
[4] A. Leong-Hoï, P. C. Montgomery, B. Serio, P. Twardowski, W. Uhring, *Opt. Lett*. **2016**, *41*, 1313.
[5] P. de Groot, *Adv. Opt. Photonics* **2015**, *7*, 1.
[6] C. S. Williams, O. A. Becklund, Introduction to the Optical Transfer Function (SPIE Press, **1989**).
[7] P. C. Montgomery, D. Montaner, *Microelectronic Engineering*, **1999**, *45*, 291.
[8] M. G. L. Gustafsson, *Proc. Natl. Acad. Sci. U. S. A*. **2005**, *102*, 13081.
[9] M. Debailleul, V. Georges, B. Simon, R. Morin, O. Haeberlé, *Opt. Lett*. **2009**, *34*, 79.
[10] Z. Chen, A. Taflove, V. Backman, *Opt. Express* **2004**, *12*, 1214.
[11] A. Heifetz, J. J. Simpson, S.-C. Kong, A. Taflove, V. Backman, *Opt. Express* **2007**, *15*, 17334.
[12] Z. Wang, W. Guo, L. Li, B. Luk'yanchuk, A. Khan, Z. Liu, Z. Chen, M. Hong, *Nat. Commun*. **2011**, *2*, 218.
[13] X. Hao, C. Kuang, X. Liu, H. Zhang, Y. Li, *Appl. Phys. Lett* **2011**, *99*, 203102.
[14] F. Wang, L. Liu, H. Yu, Y. Wen, P. Yu, Z. Liu, Y. Wang, W. J. Li, *Nat. Commun*. **2016**, *7*, 13748.
[15] F. Wang, L. Liu, P. Yu, Z. Liu, H. Yu, Y. Wang, W. J. Li, *Sci. Rep*. **2016**, *6*, 24703.
[16] I. Kassamakov, S. Lecler, A. Nolvi, A. Leong-Hoï, P. Montgomery, E. Haeggström, *Sci. Rep*. **2017**, *7*, 3683.
[17] M. Aakhte, V. Abbasian, E. A. Akhlaghi, A.-R. Moradi, A. Anand, B. Javidi, *Appl. Opt*. **2017**, *56*, D8.
[18] S. Perrin, A. Leong-Hoï, S. Lecler, P. Pfeiffer, I. Kassamakov, A. Nolvi, E. Haeggström, P. Montgomery, *Appl. Opt*. **2017**, *56*, 7249.
[19] S. Perrin, S. Lecler, A. Leong-Hoi, P. C. Montgomery, Proc. SPIE 10330 (**2017**).
[20] H. Takajo, T. Takahashi, *JOSA A* **1988**, *5*, 1818.
[21] A. Y. Vorobyev, C. Guo, *Appl. Phys. Lett*. **2008**, *92*, 41914.
[22] B. Dusser, Z. Sagan, H. Soder, N. Faure, J.-P. Colombier, M. Jourlin, E. Audouard, *Opt. Express*. **2010**, *18*, 2913.
[23] C. Hairaye, F. Mermet, T. Engel, P. C. Montgomery, J. Fontaine, *J. Phys.: Conf. Ser*. **2014**, *558*, 012063.
[24] B. Dusser, Z. Sagan, A. Foucou, M. Jourlin, E. Audouard, In SPIE LASE: Lasers and Applications in Science and Engineering 72010V (**2009**).